Electronic Supporting Information (ESI)

A Cu(I) metal-organic framework with 4-fold helical channels for sensing anions

Yong-Qiang Chen, Guo-Rong Li, Ze Chang, Yang-Kun Qu, Ying-Hui Zhang and Xian-He Bu*

Department of Chemistry, TKL of Metal- and Molecule-Based Material Chemistry and Synergetic Innovation Center of Chemical Science and Engineering (Tianjin), Nankai University, Tianjin 300071, China.

**To whom correspondence should be addressed. E-mail: buxh@nankai.edu.cn*

S1. Materials and Measurements

All the chemicals used for synthesis were of analytical grade and commercially available. The 2,4,6-tris(4-pyridyl)pyridine (pytpy) ligand was synthesized according to the reported method.[1] IR spectra were measured on a Tensor 27 OPUS (Bruker) FT-IR spectrometer with KBr pellets. Powder X-ray diffraction (PXRD) spectra were recorded on a Bruker D8 FOCUS diffractometer with a Cu-target tube and a graphite monochromator. Thermogravimetric (TG) analyses were carried out on a Rigaku standard TG-DTA analyzer with a heating rate of 10°C min^{-1} from ambient temperature to 800°C under nitrogen gas. Gas adsorption measurements were performed using an ASAP 2020 M gas adsorption analyzer. UHP-grade gases were used in measurements. Fluorescence spectra were performed on a Hitachi F-4500 fluorescence/phosphorescence spectrophotometer at room temperature. XPS spectra were obtained from PHI5000VersaProbe. Solid state ^{13}C NMR spectra were measured on a Varian Infinityplus-400 spectrometer. Field emission SEM and EDX were conducted by using a SU-8010 scanning electron microscope. Ion chromatography (IC) was obtained from IC-2011 ion chromatograph.

S2. Experiment Details

Synthesis of $\{[Cu(pytpy)]\cdot NO_3\cdot CH_3OH\}_\infty$ (1). A mixture of $Cu(NO_3)_2\cdot 3H_2O$ (72 mg, 0.3 mmol), pytpy (31 mg, 0.1 mmol) in 10 mL mixed solvent ($V_{N,N\text{-}dimethyl\ acetamide} : V_{methanol} = 1 : 1$) was sealed in a Teflon-lined autoclave and heated to 120 °C for 3 days. After the autoclave was cooled to room temperature at 10 °C h^{-1}, orange block crystals were collected by filtration, and washed with 3 × 10 mL

of methanol and then air-dried. Yield: ~60% based on pytpy. Anal. Calcd for $C_{21}H_{18}N_5O_4Cu$: C, 53.90; H, 3.88; N, 14.97%. Found: C, 53.62; H, 3.47; N, 15.08%. IR (KBr, cm^{-1}): 3554m, 3075m, 2356w, 1603s, 1534s, 1500m, 1370s, 1329s, 1220m, 1055s, 1021w, 822s, 630s, 521s.

{[Cu(pytpy)]·NO_3·H_2O}$_\infty$ (1'). When complex **1** was allowed to stand at room temperature over one week or heated at atmosphere for *ca.* 2 h under ambient humidity, the guest methanol molecules were exchanged by water molecules, and a single-crystal-to-single-crystal (SC–SC) transformation took place, and complex **1'** was formed. Anal. Calcd for $C_{20}H_{16}N_5O_4Cu$: C, 52.92; H, 3.55; N, 15.43%. Found: C, 53.16; H, 3.27; N, 15.68%. IR (KBr, cm^{-1}): 3546m, 3066m, 2398w, 1594s, 1534s, 1500m, 1368s, 1334s, 1224m, 1055s, 1012w, 815s, 626s, 516s.

{[Cu(pytpy)]·NO_3·CH_3OH }$_\infty$ (1a). When the hydrated complex **1'** was immersed in anhydrous methanol for over 3 h, the guest water molecules in the channel were exchanged by methanol molecules again, and complex **1a** was obtained. Anal. Calcd for $C_{21}H_{18}N_5O_4Cu$: C, 53.90; H, 3.88; N, 14.97%. Found: C, 53.46; H, 3.97; N, 14.68%. IR (KBr, cm^{-1}): 3542m, 3068m, 2408w, 1597s, 1534s, 1500m, 1371s, 1332s, 1223m, 1055s, 1018w, 819s, 626s, 520s.

S3. X-ray Data Collection and Structure Determinations.

X-ray single-crystal diffraction data of **1**, **1'** and **1a** were collected on a Rigaku SCX-mini diffractometer with graphite monochromatic Mo-Kα radiation (λ = 0.71073 Å). The program CrystalClear was used for integration of the diffraction profiles. All the structures were solved by direct methods using the SHELXS program of the SHELXTL package and refined by full-matrix least-squares methods with SHELXL.[2] Metal atoms were located from the *E*-maps and other non-hydrogen atoms excluded in conterions were located in successive difference Fourier syntheses and refined with anisotropic thermal parameters on F^2. Further details of crystal data and structure refinement for **1**, **1'** and **1a** were summarized in Table S1. CCDC 910726 – 910728.

Reference:

1. C. Liu, Y. B. Ding, X. H. Shi, D. Zhang, M. H. Hu, Y. G. Yin and D. Li, *Cryst. Growth Des.*, 2009, **9**, 1275.

2. Sheldrick, G. M. *SHELXTL NT Version 5.1. Program for Solution and Refinement of Crystal Structures,* University of Göttingen, Germany, 1997.

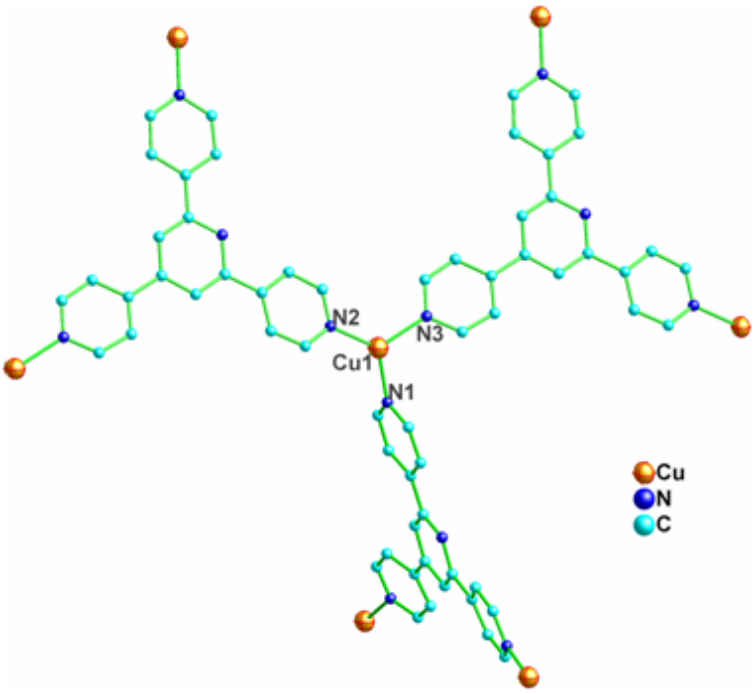

Figure S1. The coordination environment of Cu(I) in **1**.

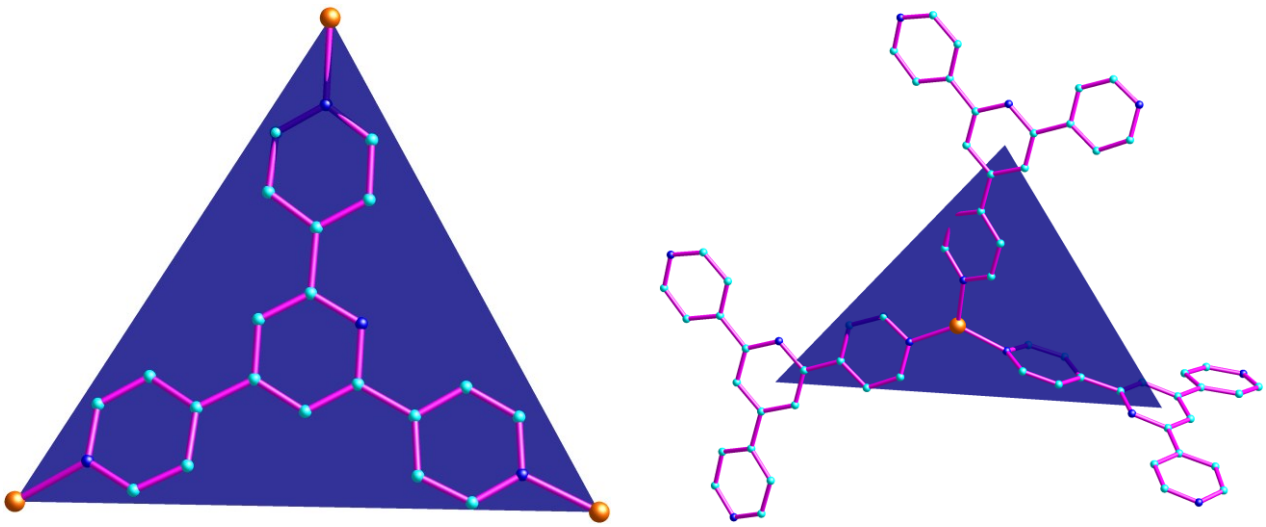

(a) (b)

Figure S2. View of the connection modes of pytpy and Cu(I) ion.

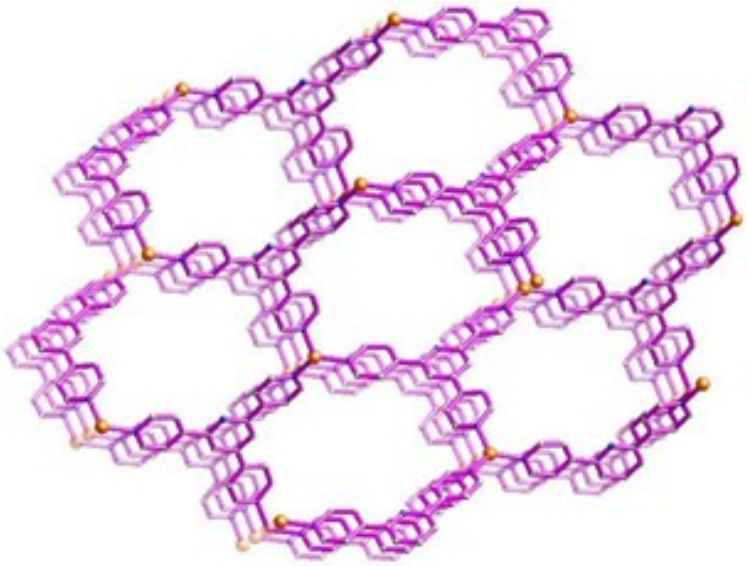

Figure S3. The single (10,3)-b network in **1**.

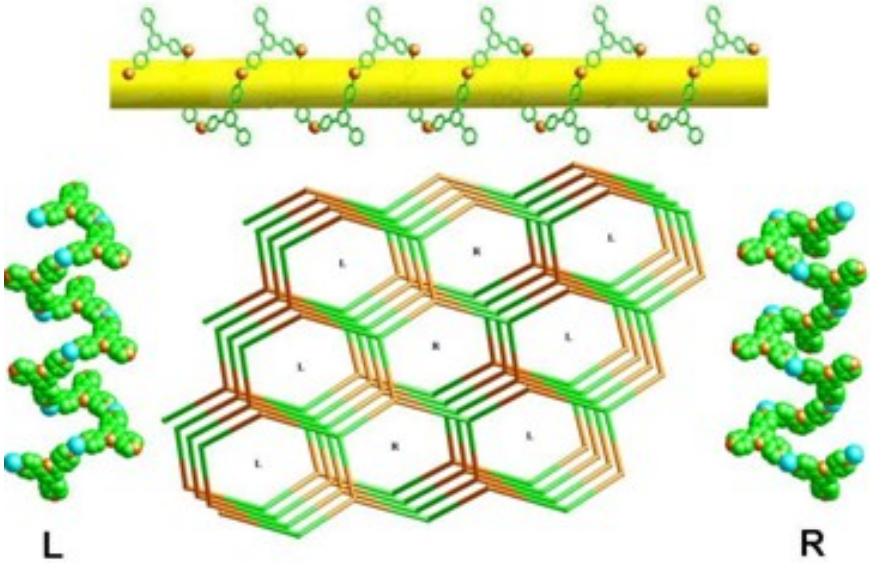

Figure S4. The (10,3)-b topology with the right- and left-handed hexagonal helices in **1**.

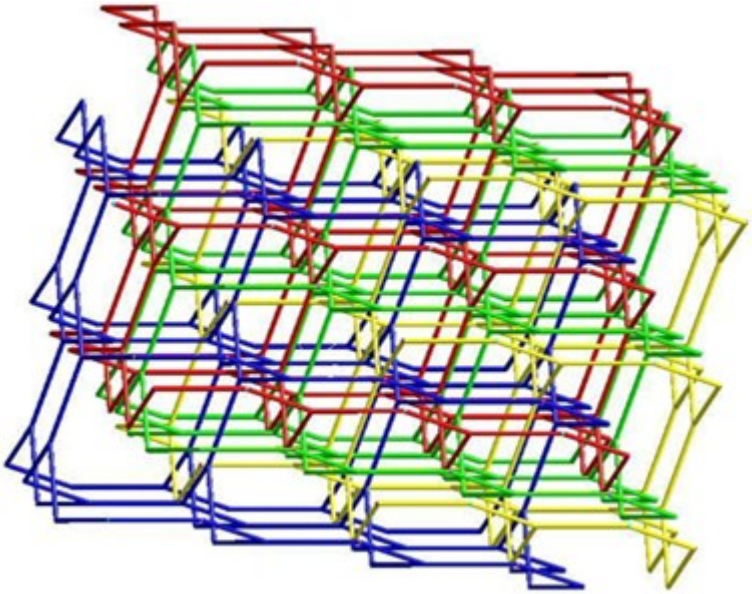

Figure S5. The 4-fold interpenetrating framework of **1**.

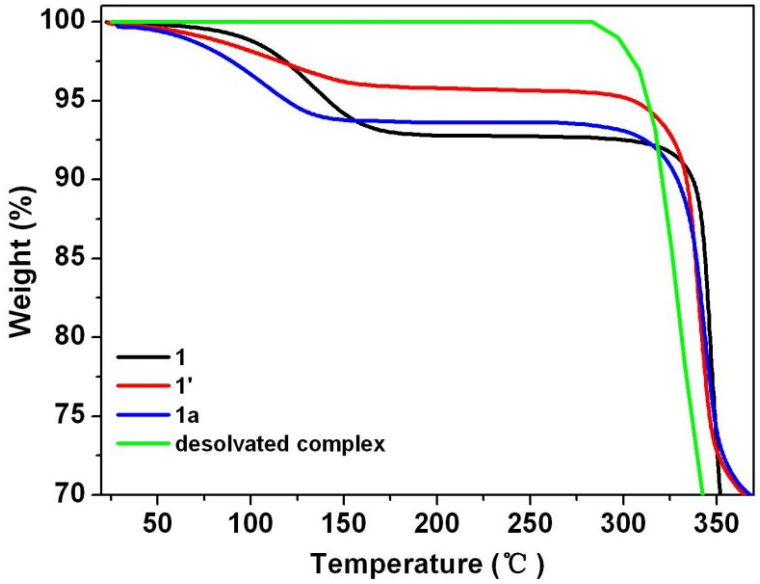

Figure S6. The thermogravimetric (TG) curves of **1** (black line), **1'** (red line), **1a** (blue line) and the desolvated complex (green line) below 375 °C.

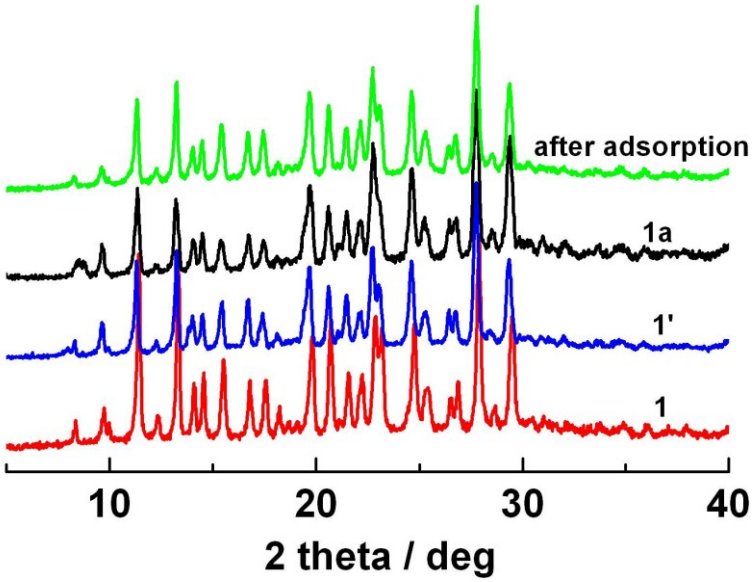

Figure S7. The PXRD patterns of complexes **1**, **1'**, **1a**, and the activated complex after adsorption.

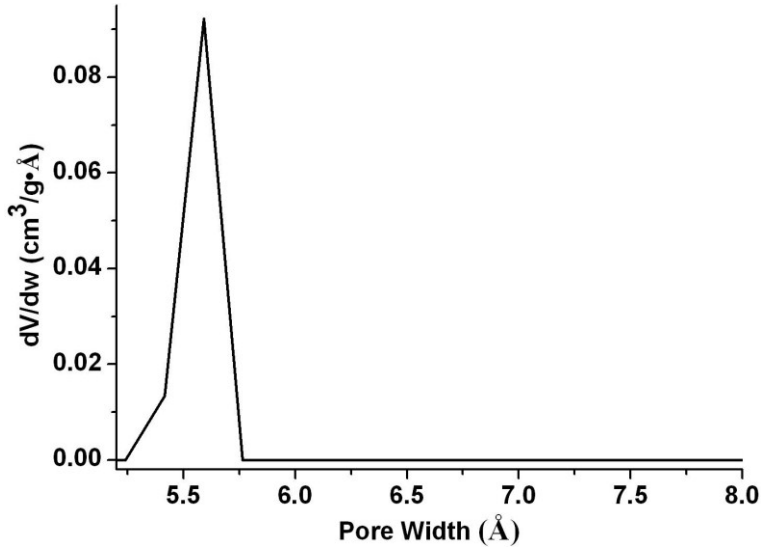

Figure S8. Pore size distribution of the activated complex **1** using DFT mode, based on CO_2 adsorption data at 273 K.

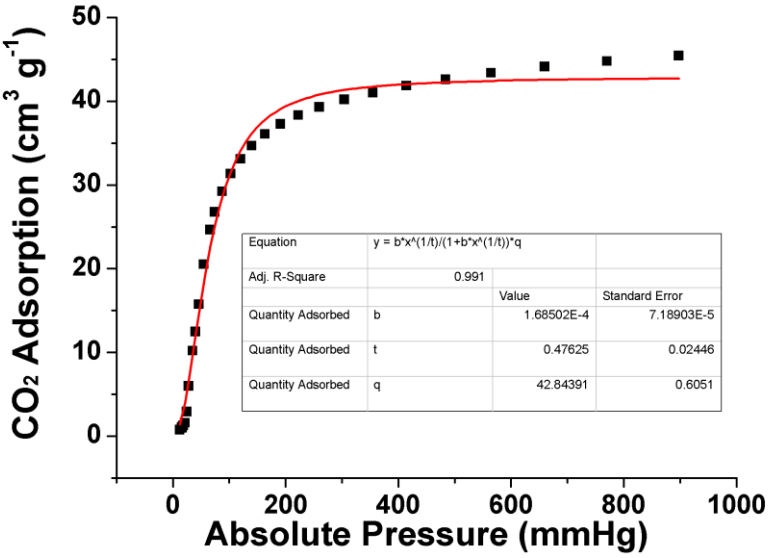

Figure S9. CO_2 adsorption isotherm for complex **1** at 273 K. The solid line represents the best fit to the data using the Langmuir-Freundlich equation.

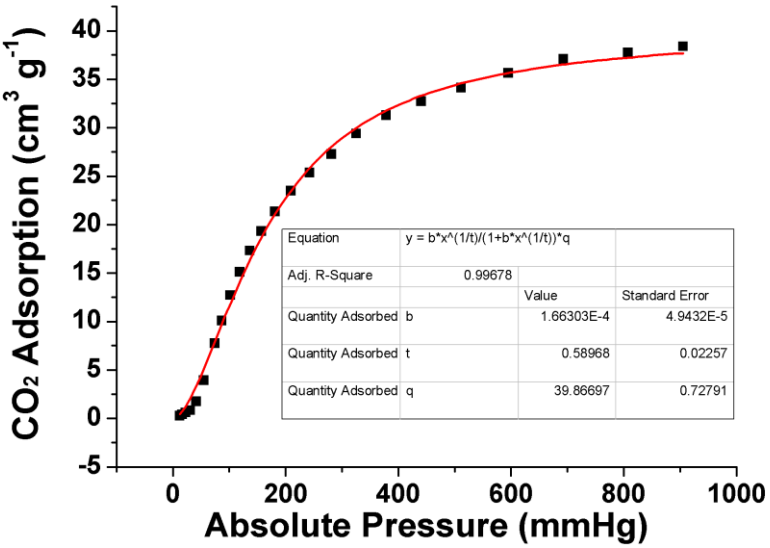

Figure S10. CO_2 adsorption isotherm for complex **1** at 298 K. The solid line represents the best fit to the data using the Langmuir-Freundlich equation.

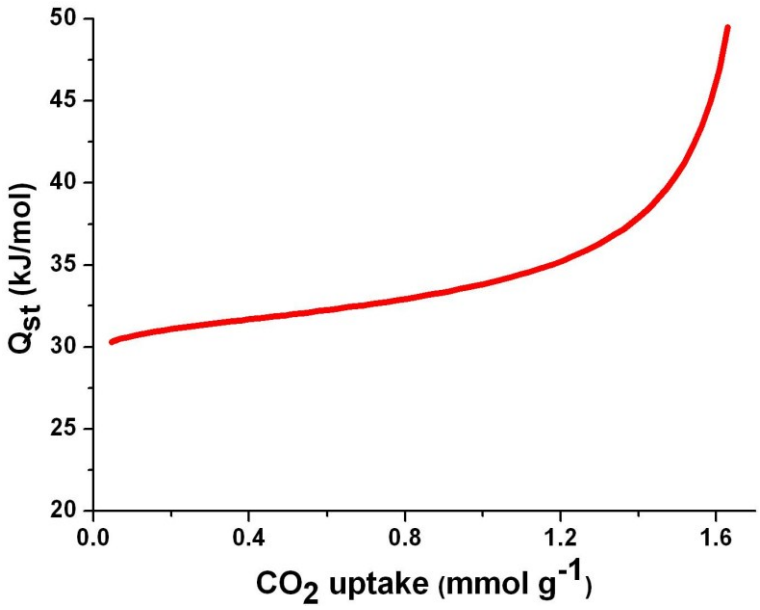

Figure S11. Isosteric heat of CO_2 adsorption.

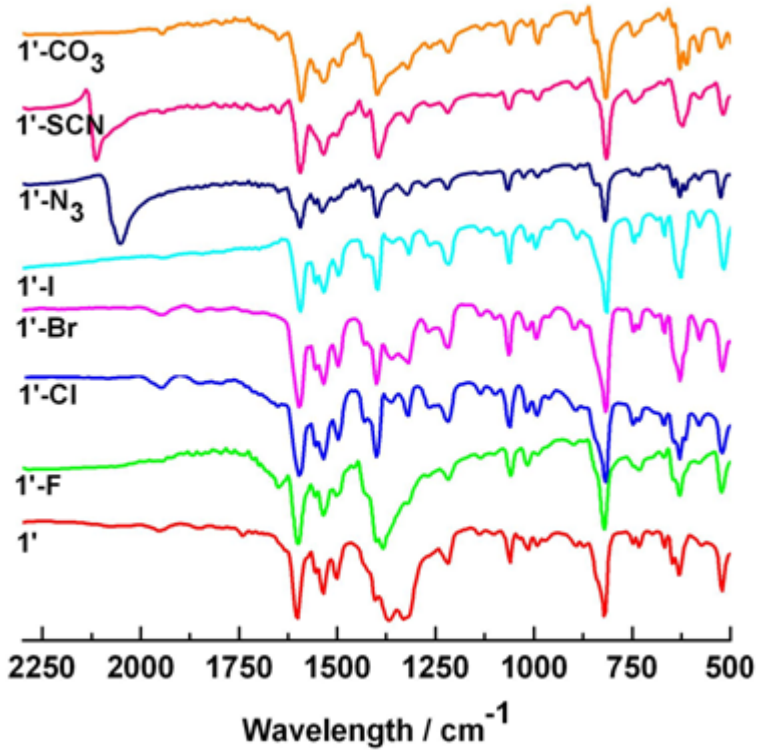

Figure S12. IR spectra of complex **1'** and the anion-exchanged complexes.

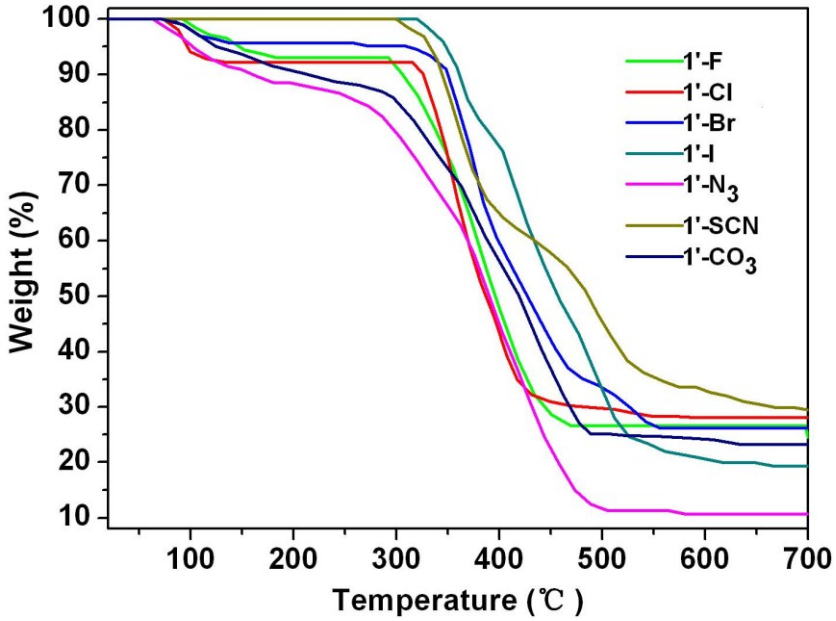

Figure S13. The thermogravimetric (TG) curves of the anion-exchanged complexes.

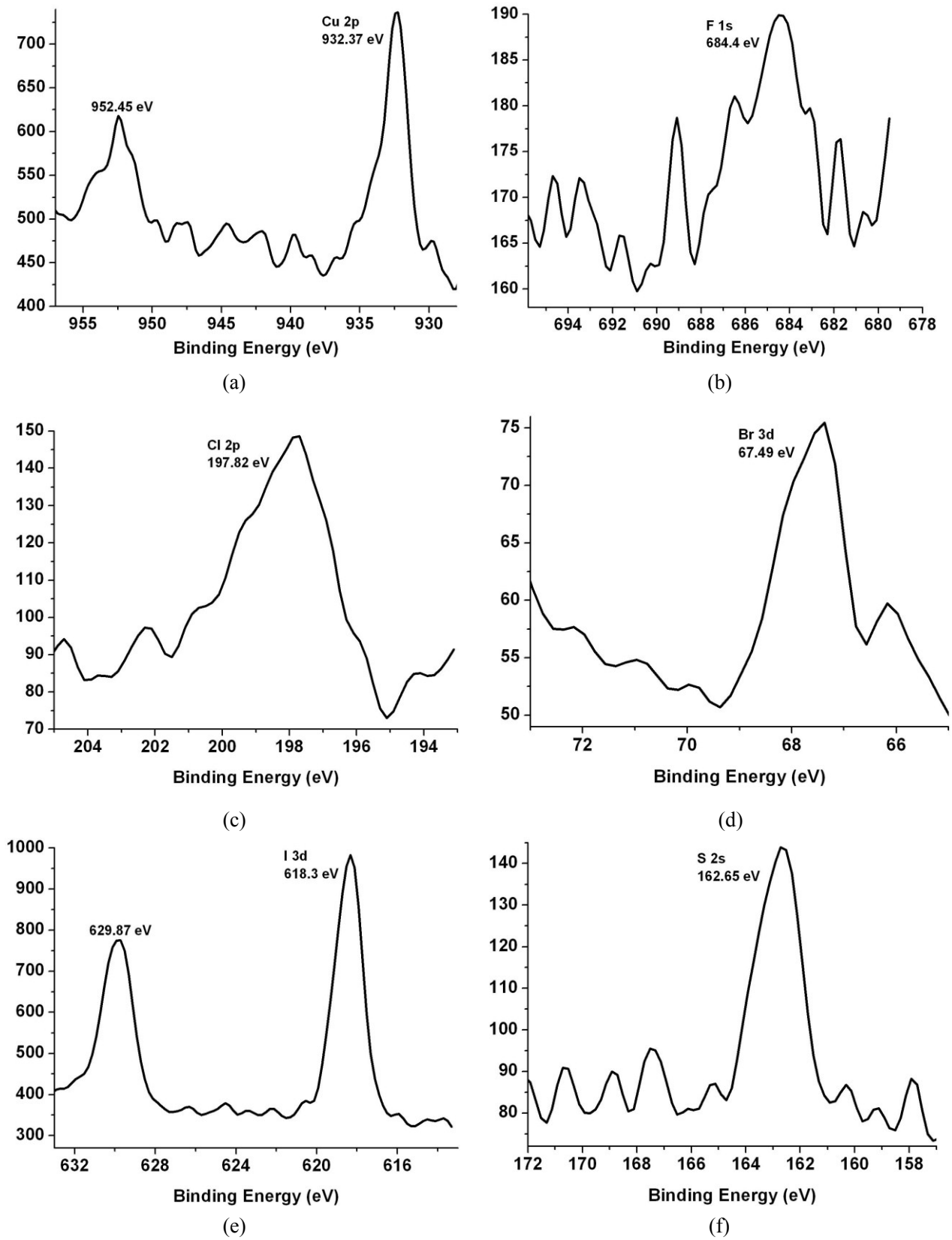

Figure S14. XPS spectra of **1**(a), **1'**-F (b), **1'**-Cl (c), **1'**-Br (d), **1'**-I (e), and **1'**-SCN (f).

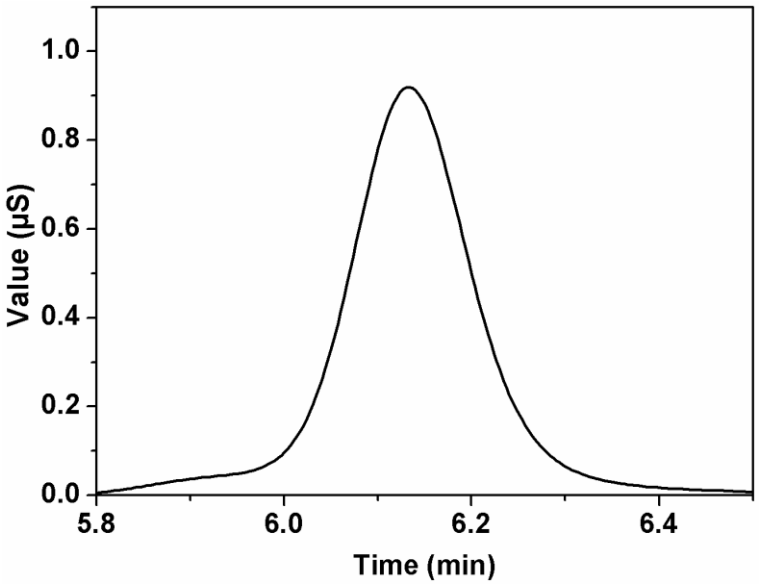

Figure S15. Chromatogram of NO_3^- anion in standard solution separated by the column-switching IC system for solution of complex **1'**-F. Injection volume: 25 μL，EGC-KOH eluent generator.

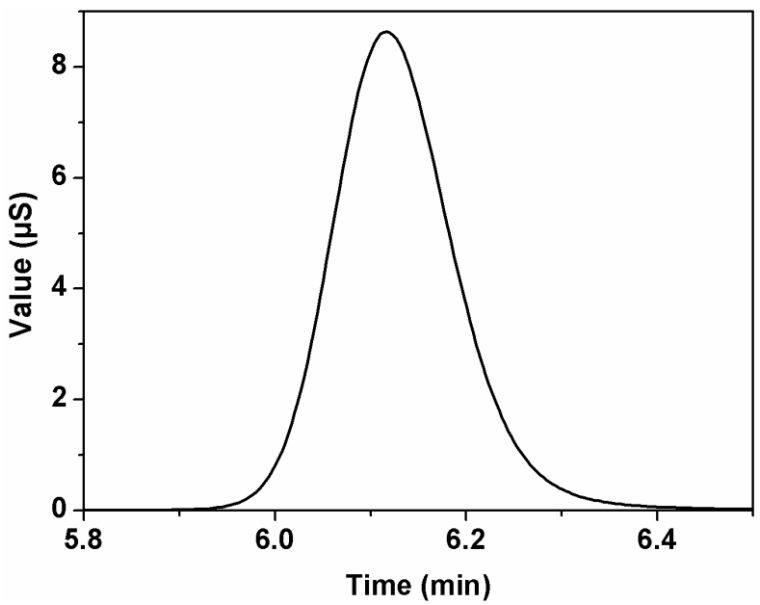

Figure S16. Chromatogram of NO_3^- anion in standard solution separated by the column-switching IC system for solution of complex **1'**-Cl. Injection volume: 25 μL，EGC-KOH eluent generator.

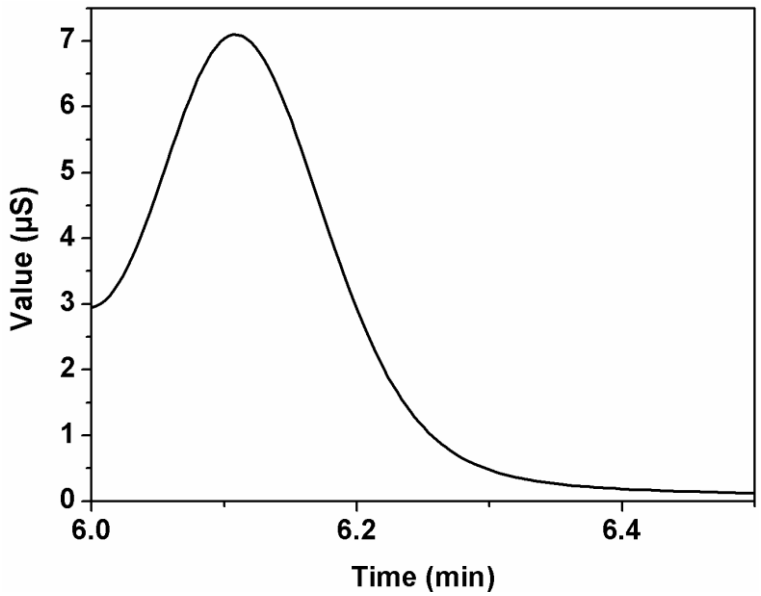

Figure S17. Chromatogram of NO_3^- anion in standard solution separated by the column-switching IC system for solution of complex **1'**-Br. Injection volume: 25 μL，EGC-KOH eluent generator.

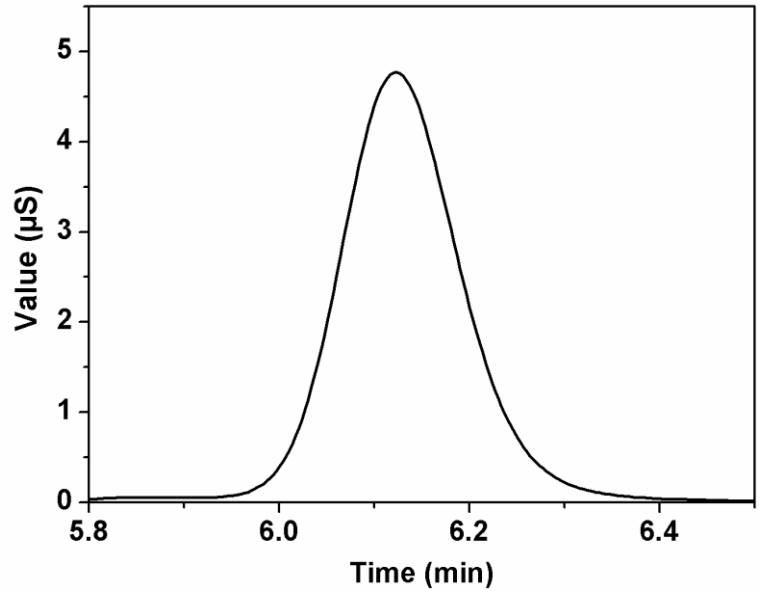

Figure S18. Chromatogram of NO_3^- anion in standard solution separated by the column-switching IC system for solution of complex **1'**-I. Injection volume: 25 μL，EGC-KOH eluent generator.

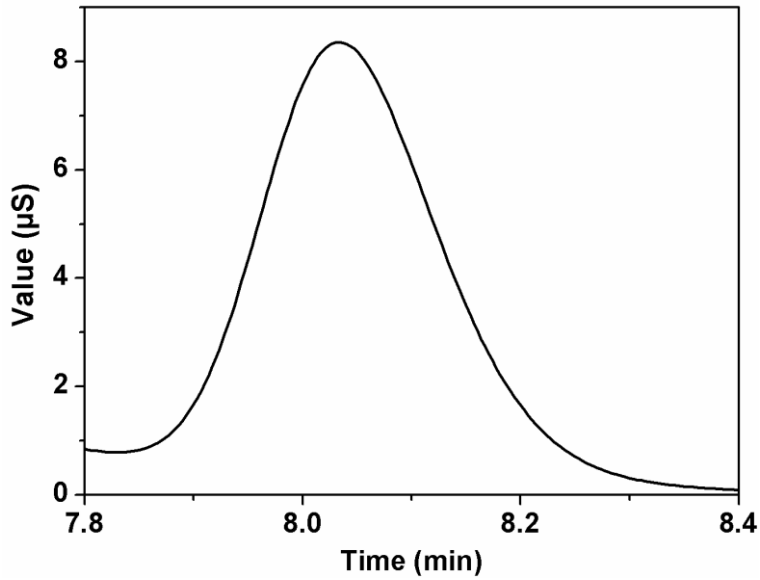

Figure S19. Chromatogram of NO_3^- anion in standard solution separated by the column-switching IC system for solution of complex **1'**-N_3. Injection volume: 25 μL，EGC-KOH eluent generator.

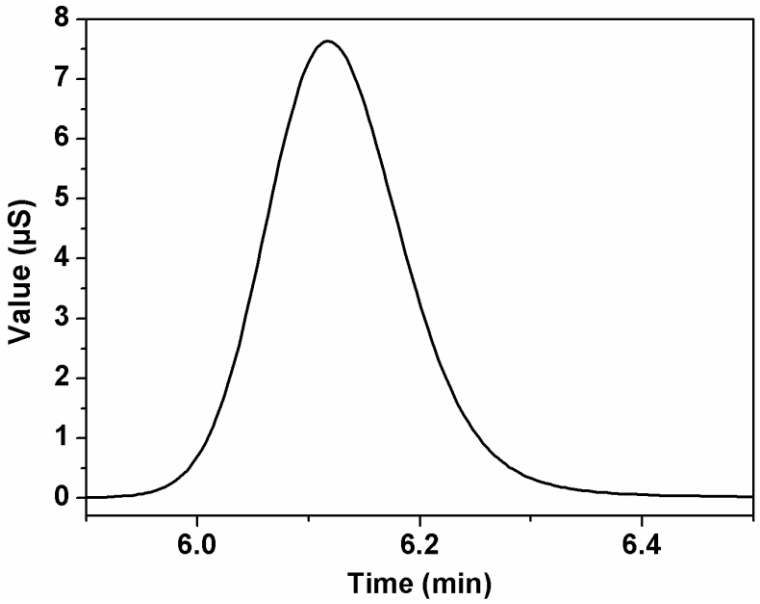

Figure S20. Chromatogram of NO_3^- anion in standard solution separated by the column-switching IC system for solution of complex **1'**-SCN. Injection volume: 25 μL，EGC-KOH eluent generator.

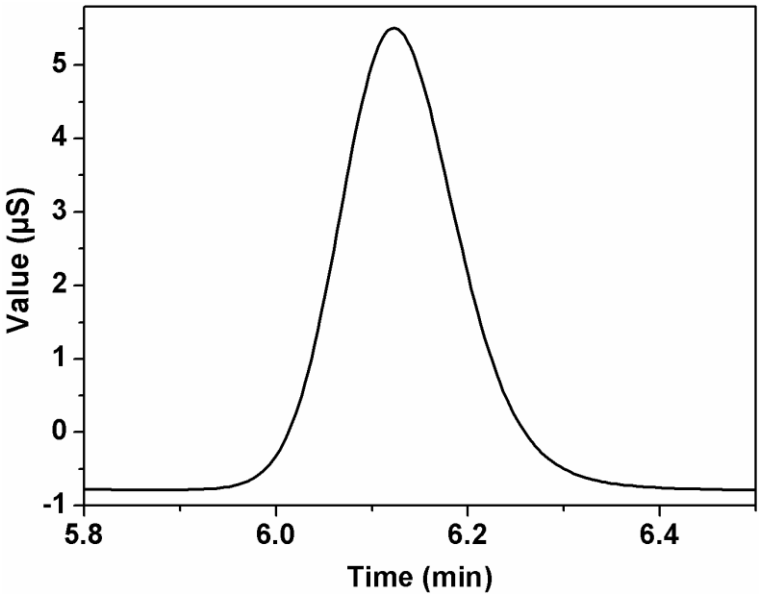

Figure S21. Chromatogram of NO_3^- anion in standard solution separated by the column-switching IC system for solution of complex **1'**-CO_3. Injection volume: 25 μL，EGC-KOH eluent generator.

The analytical results for NO_3^- anion in solution after anion exchange by the IC measurements

Complexes	Time Min NO_3^-	Peak area μS*min NO_3^-	Peak height μS NO_3^-	Concentration ppm NO_3^-
1'-F	6.134	0.1543	0.93	0.8241
1'-Cl	6.117	1.3123	8.63	7.7719
1'-Br	6.107	1.0443	6.64	6.1643
1'-I	6.124	0.7224	4.76	4.2326
1'-N_3	8.034	1.7682	8.35	10.1189
1'-SCN	6.117	1.1529	7.63	6.8305
1'-CO_3	6.124	0.9579	6.31	5.6455

The SEM of the complex 1' and anion-exchanged complexes

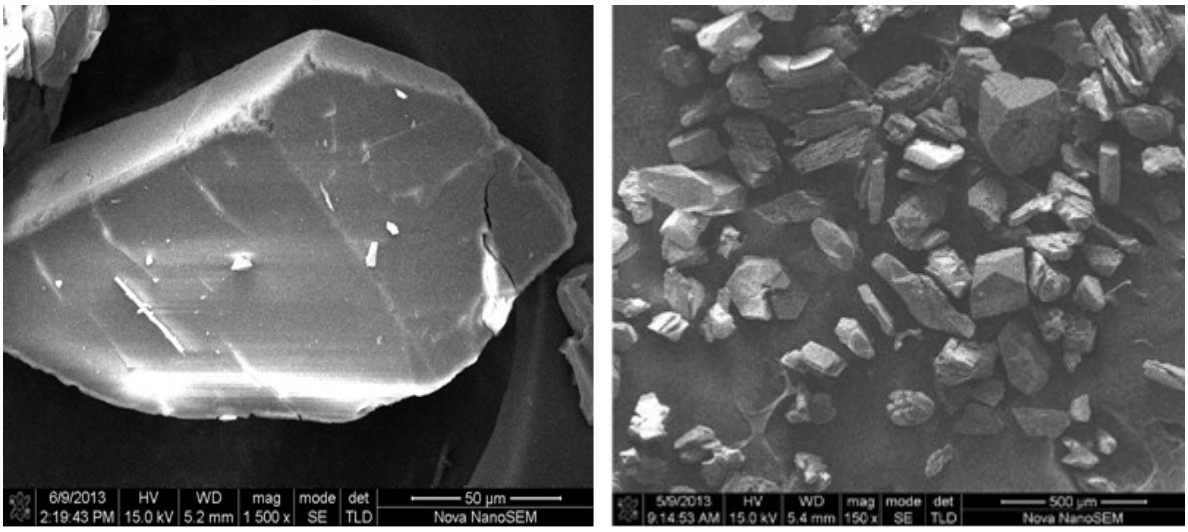

Figure S22. SEM images of complex **1'** at different magnification.

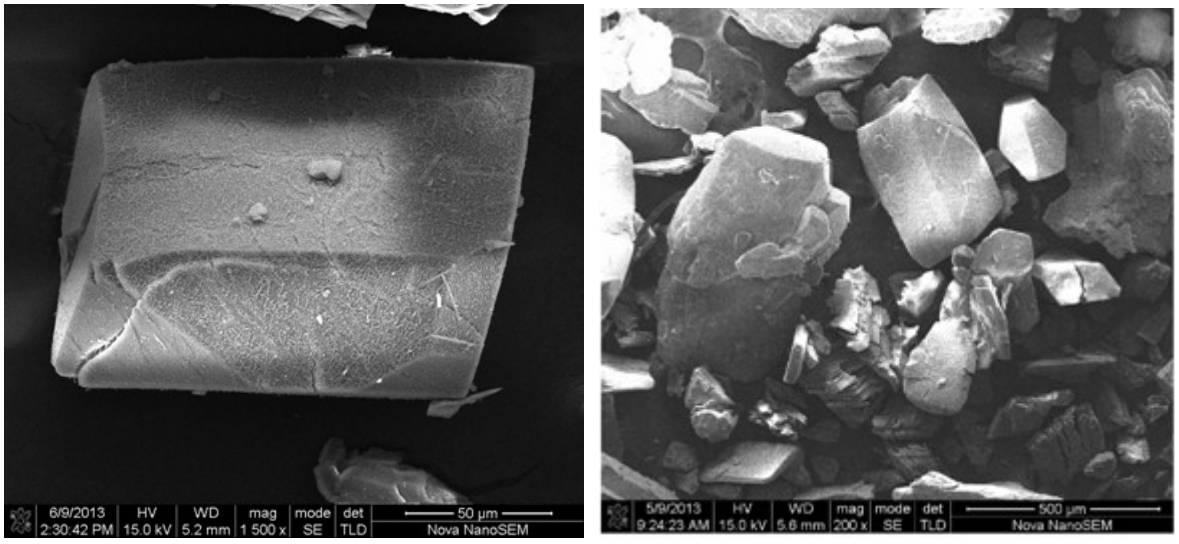

Figure S23. SEM images of complex **1'**-F at different magnification.

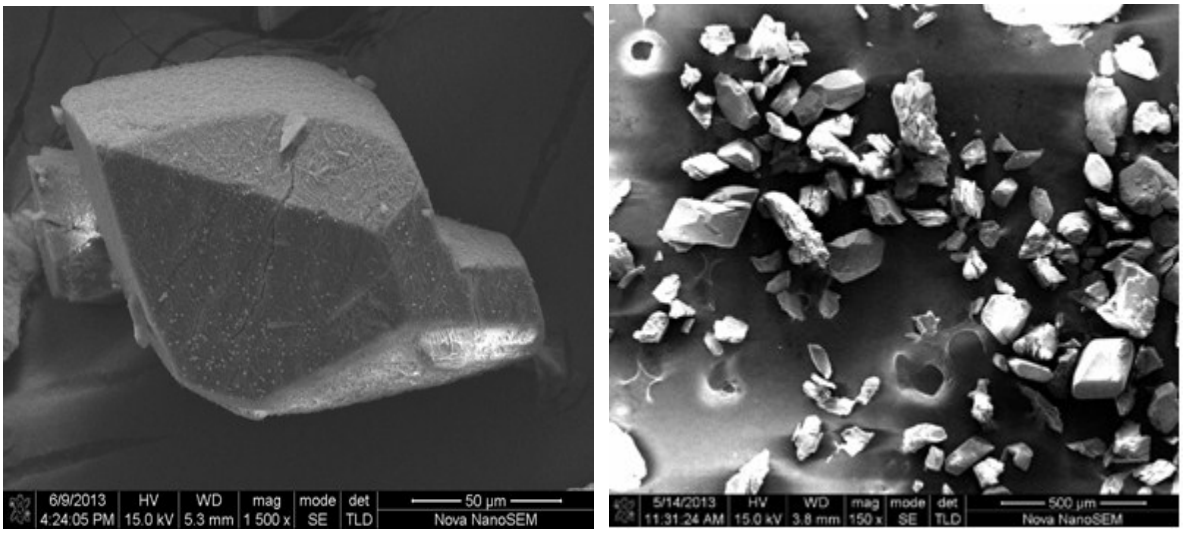

Figure S24. SEM images of complex **1'**-Cl at different magnification.

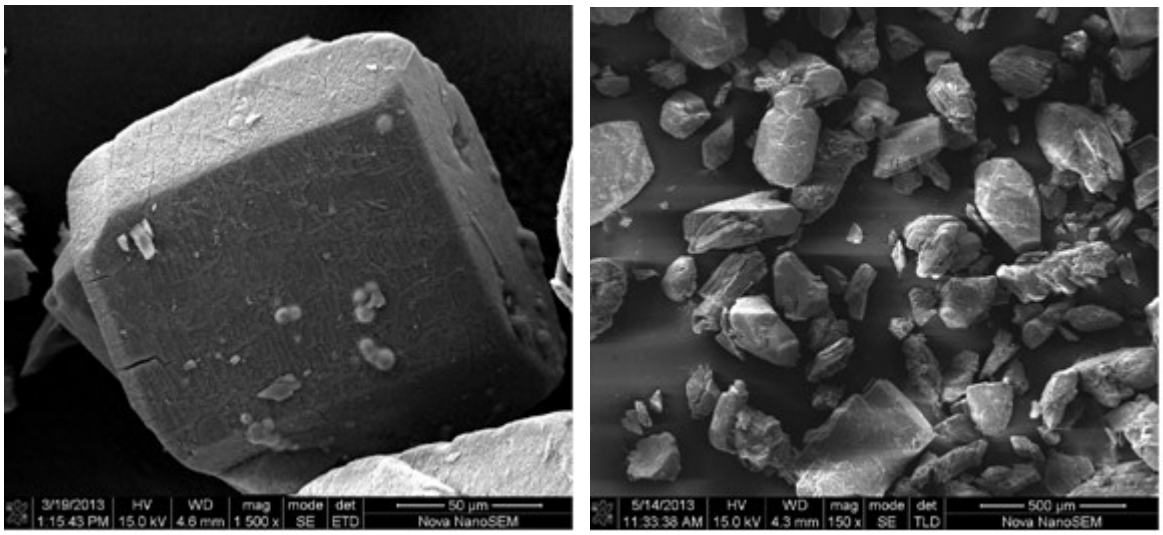

Figure S25. SEM images of complex **1'**-Br at different magnification.

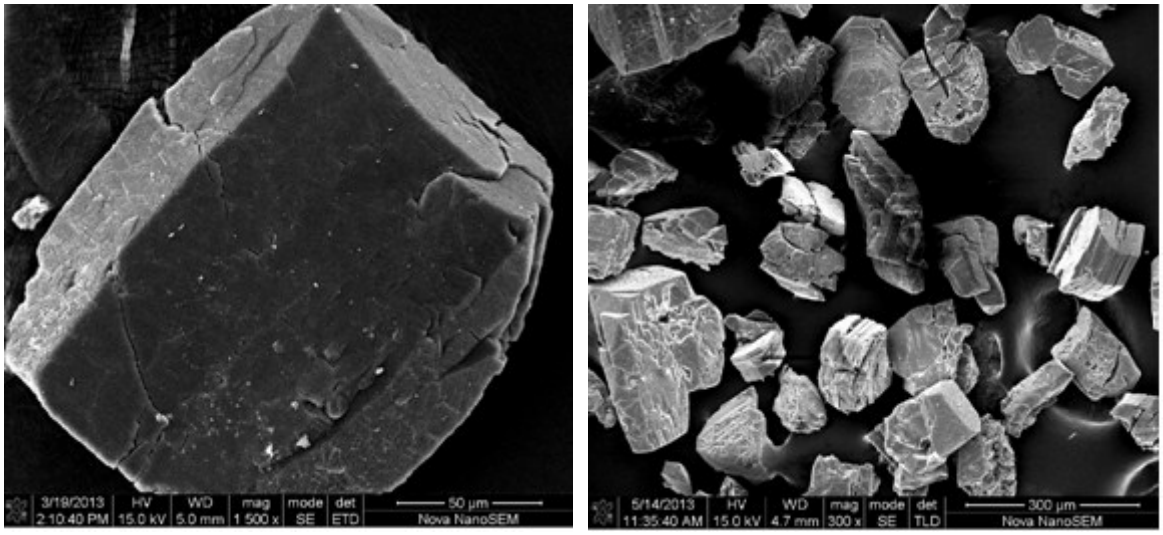

Figure S26. SEM images of complex **1'**-I at different magnification.

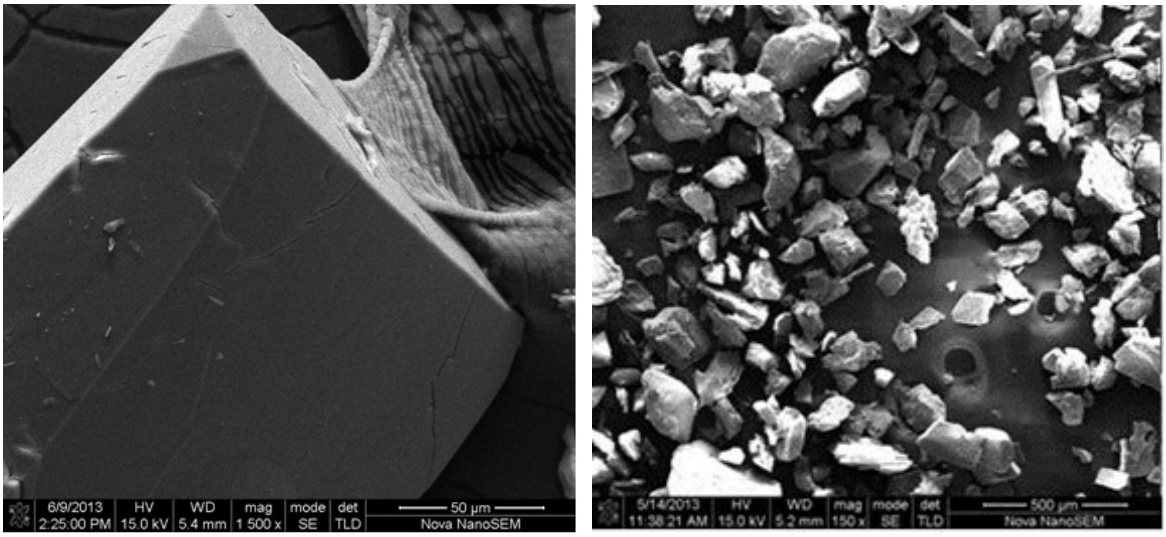

Figure S27. SEM images of complex **1'**-N_3 at different magnification.

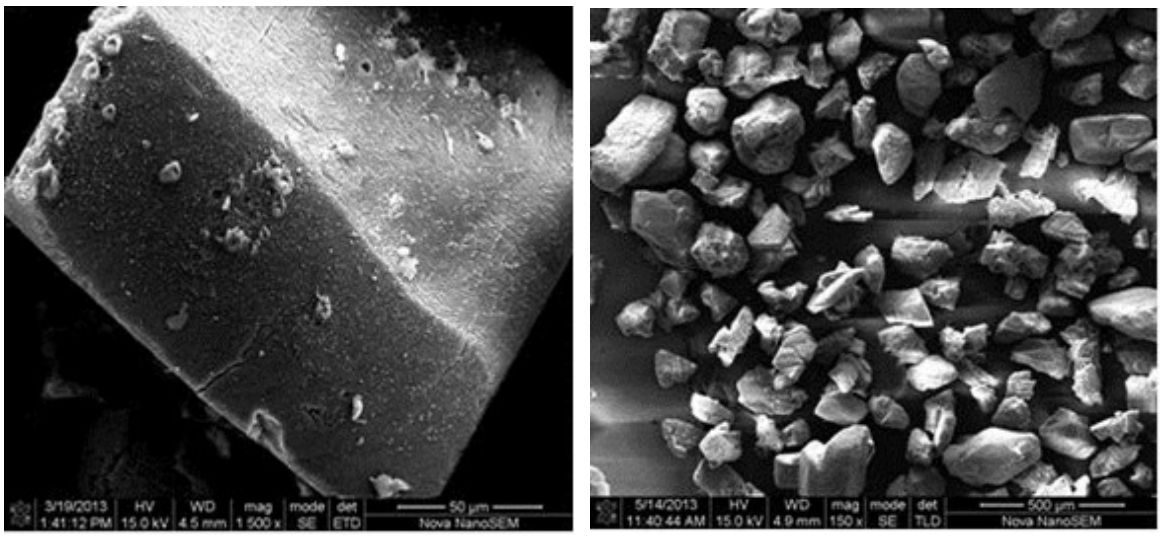

Figure S28. SEM images of complex **1'**-SCN at different magnification.

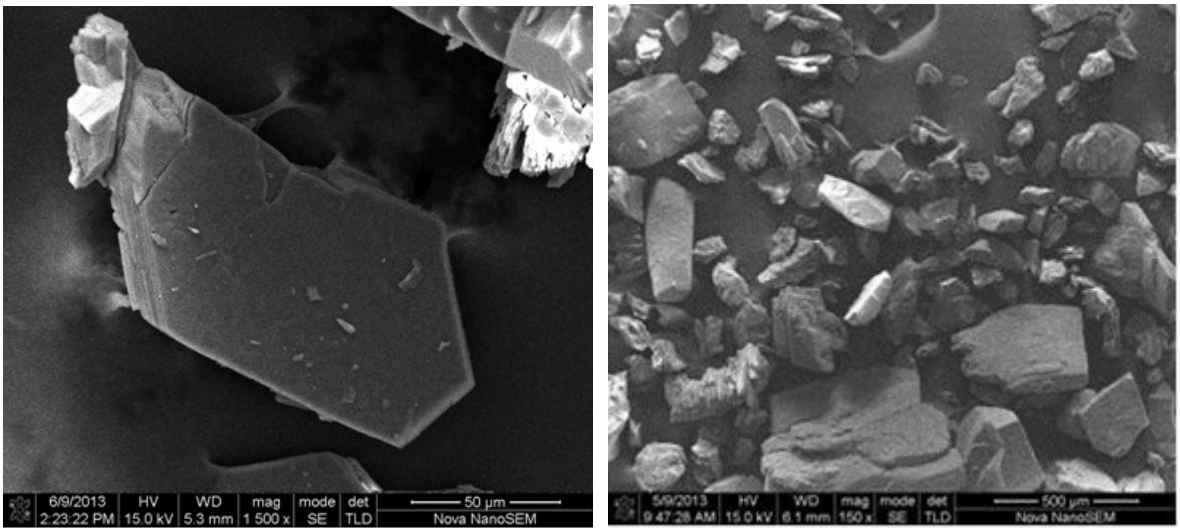

Figure S29. SEM images of complex **1'**-CO_3 at different magnification.

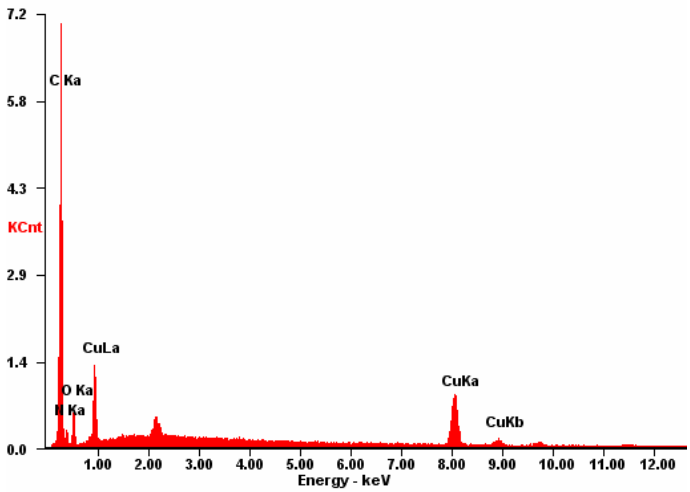

Element	*Wt%*	*At%*
CK	66.66	75.88
NK	13.41	13.09
OK	10.55	09.01
CuK	09.39	02.02
Matrix	Correction	ZAF

Figure S30. EDX of complex **1'**.

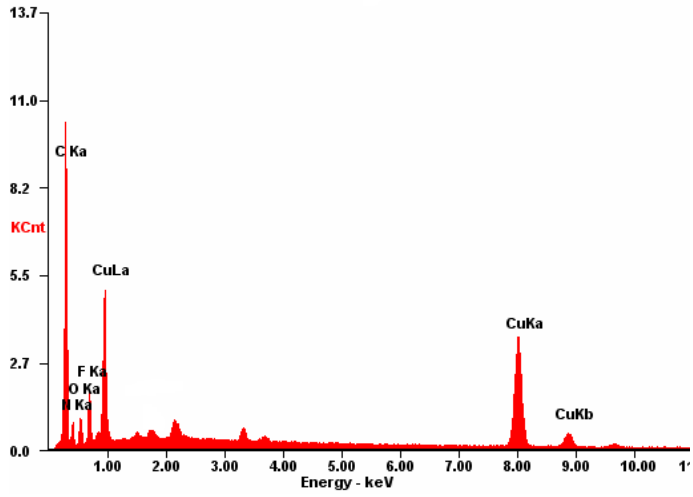

Element	*Wt%*	*At%*
CK	57.20	72.50
NK	11.89	12.92
OK	05.83	05.55
FK	04.68	03.75
CuK	16.00	03.76
Matrix	Correction	ZAF

Figure S31. EDX of complex **1'**-F.

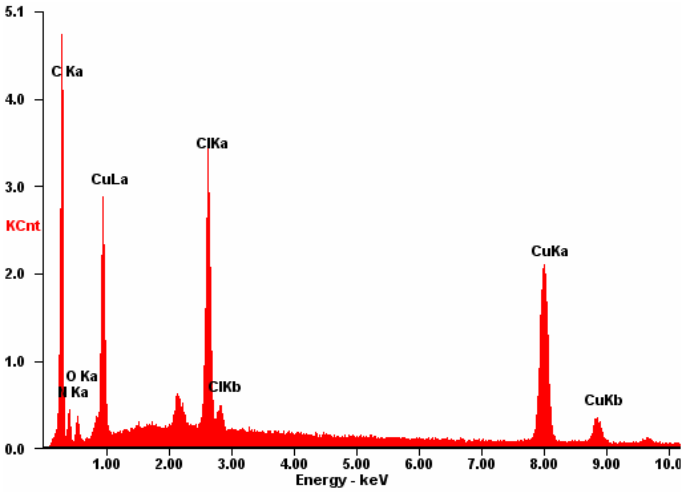

Element	*Wt%*	*At%*
CK	61.37	76.59
NK	12.77	13.67
OK	03.72	03.49
ClK	05.54	02.34
CuK	16.59	03.91
Matrix	Correction	ZAF

Figure S32. EDX of complex **1'**-Cl.

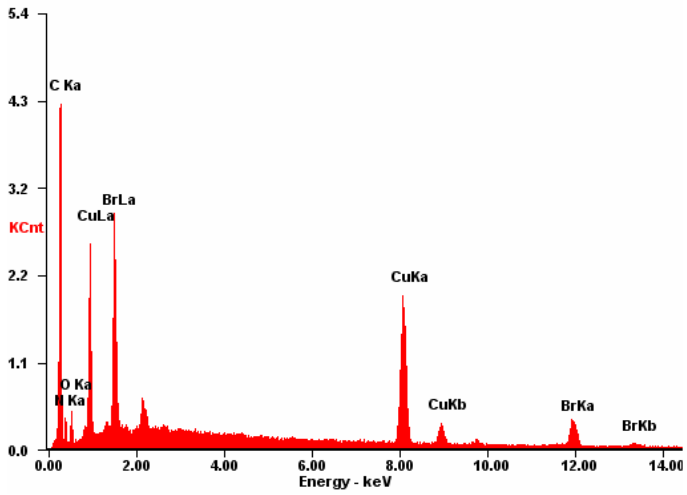

Element	*Wt%*	*At%*
CK	60.62	77.72
NK	11.16	12.27
OK	04.99	04.80
BrK	08.46	01.63
CuK	14.78	03.58
Matrix	Correction	ZAF

Figure S33. EDX of complex **1'**-Br.

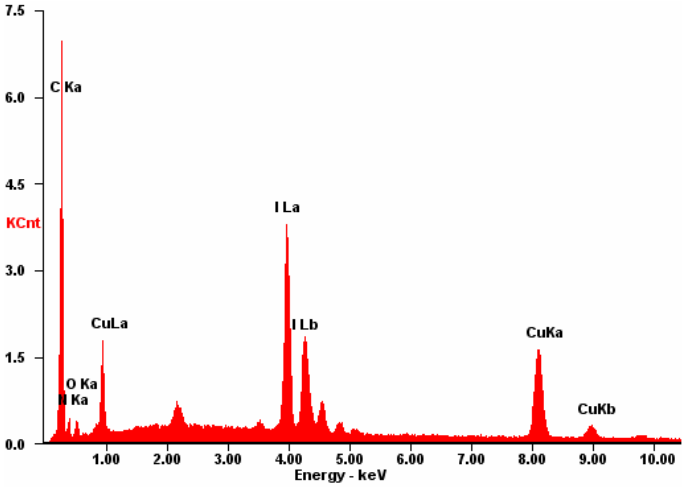

Element	*Wt%*	*At%*
CK	55.75	80.37
NK	08.38	10.36
OK	02.88	03.12
IL	20.86	02.85
CuK	12.13	03.31
Matrix	Correction	ZAF

Figure S34. EDX of complex **1'**-I.

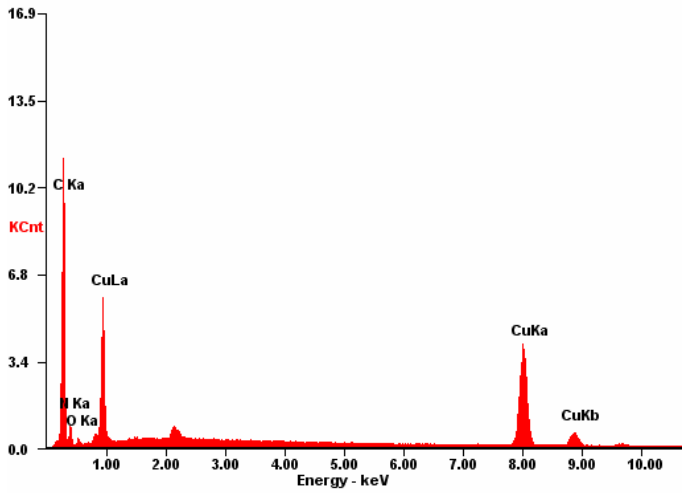

Element	*Wt%*	*At%*
CK	61.39	75.21
NK	17.81	18.71
OK	01.83	01.68
CuK	18.98	04.40
Matrix	Correction	ZAF

Figure S35. EDX of complex **1'**-N_3.

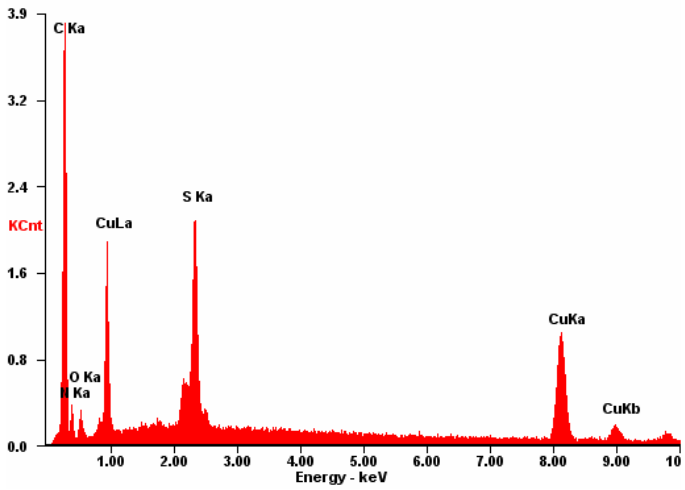

Element	*Wt%*	*At%*
CK	65.29	76.95
NK	14.57	14.73
OK	04.34	03.84
SK	04.38	01.93
CuK	11.43	02.55
Matrix	Correction	ZAF

Figure S36. EDX of complex **1'**-SCN.

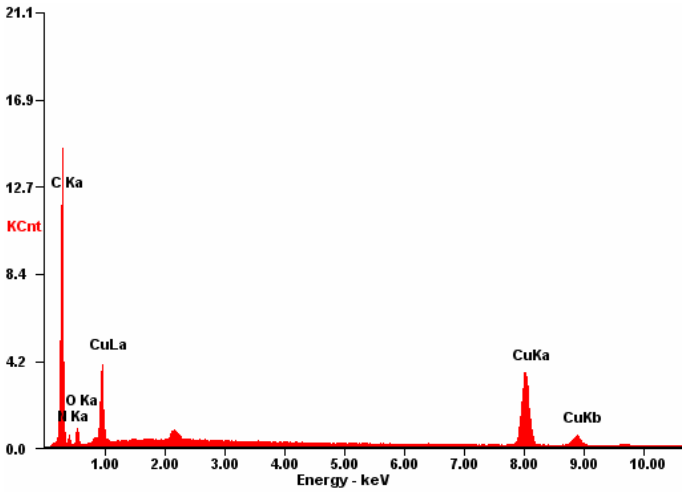

Element	*Wt%*	*At%*
CK	68.04	81.14
NK	09.78	10.00
OK	05.76	05.16
CuK	16.42	03.70
Matrix	Correction	ZAF

Figure S37. EDX of complex **1'**-CO_3.

The optical microscopy images of complex 1' and anion-exchanged complexes

Figure S38. Optical microscopy images of complex **1'**.

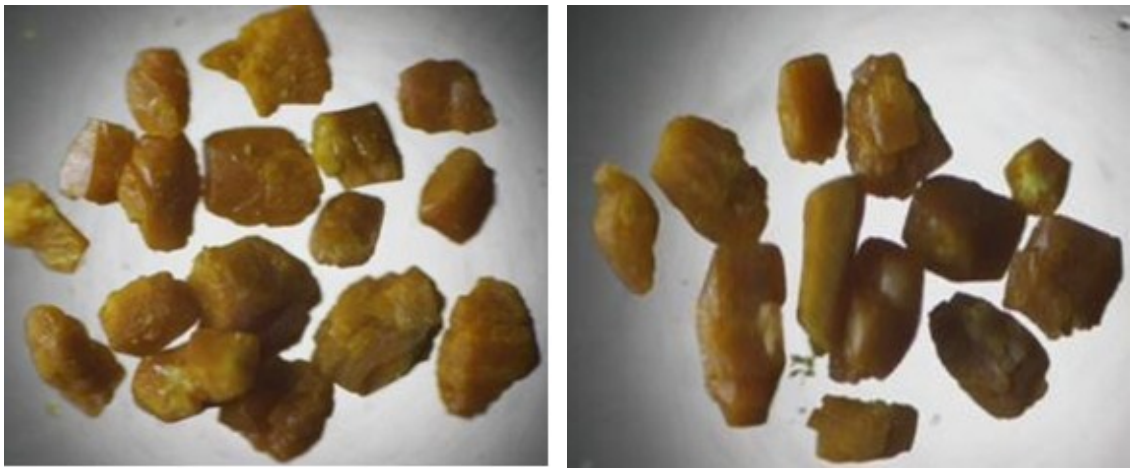

Figure S39. Optical microscopy images of complex **1'-**F (left, after 36 h; right, after 72 h).

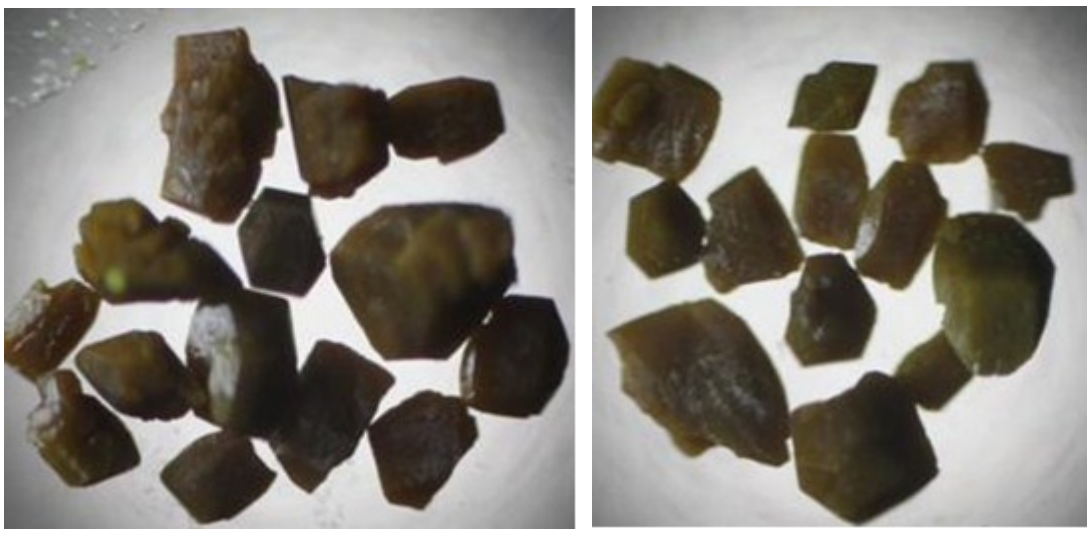

Figure S40. Optical microscopy images of complex **1'-**Cl (left, after 36 h; right, after 72 h).

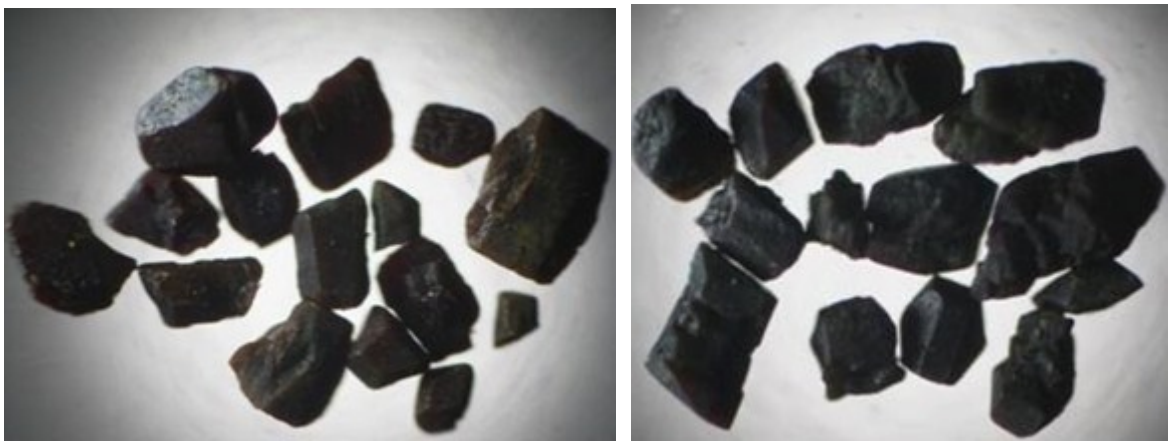

Figure S41. Optical microscopy images of complex **1'-**Br (left, after 36 h; right, after 72 h).

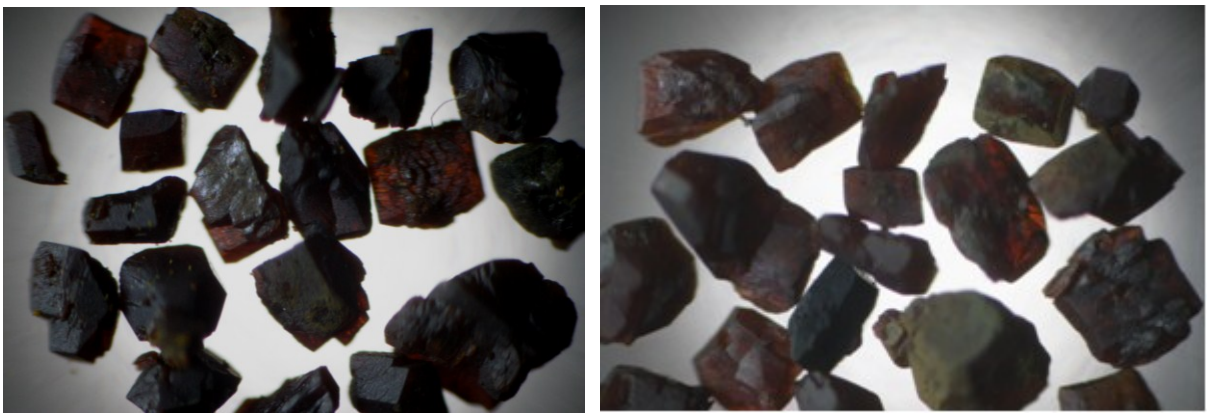

Figure S42. Optical microscopy images of complex **1'-**I (left, after 36 h; right, after 72 h).

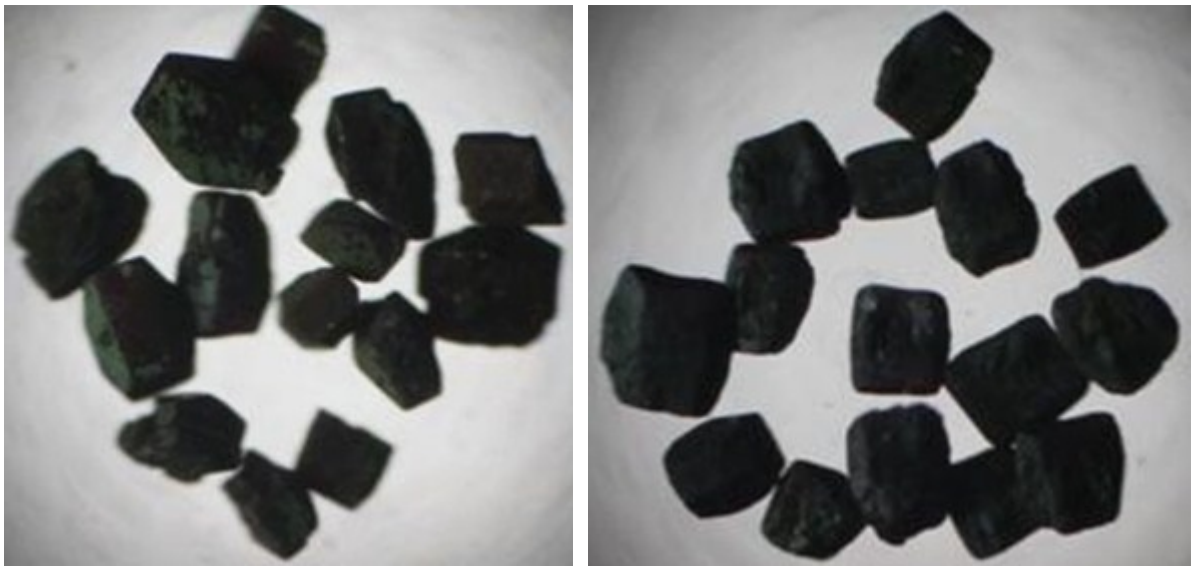

Figure S43. Optical microscopy images of complex **1'-**N_3 (left, after 36 h; right, after 72 h).

Figure S44. Optical microscopy images of complex **1'-**SCN (left, after 36 h; right, after 72 h).

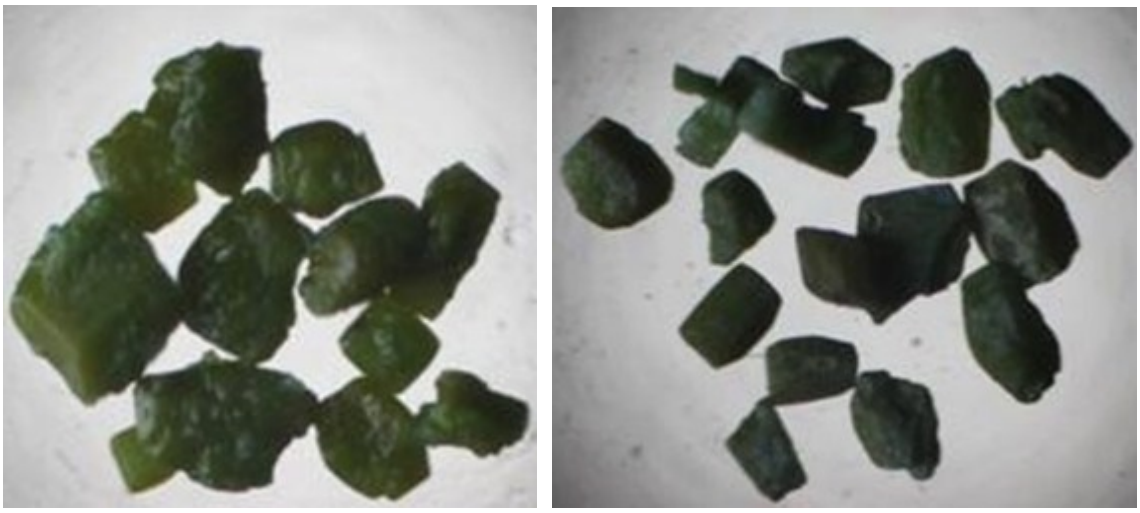

Figure S45. Optical microscopy images of complex **1'-**CO_3 (left, after 36 h; right, after 72 h).

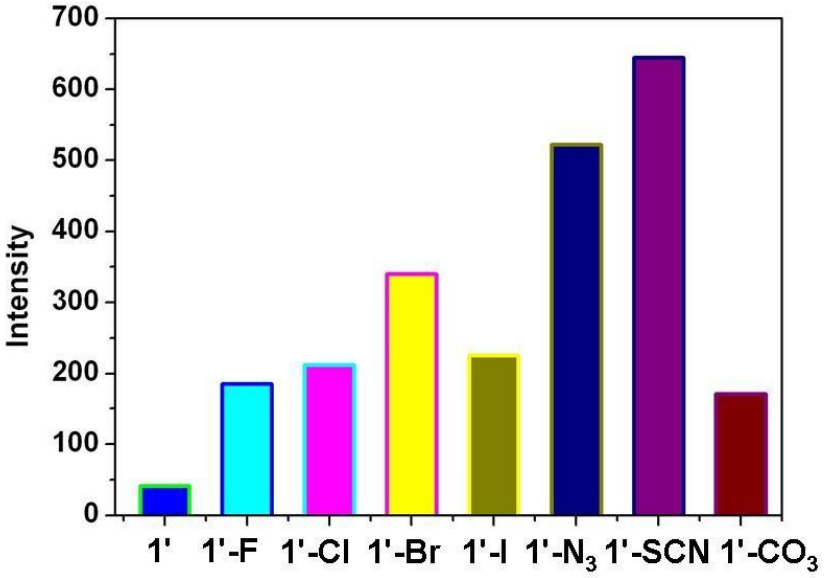

Figure S46. The emission intensities of complex **1'** and the anion-exchanged complexes.

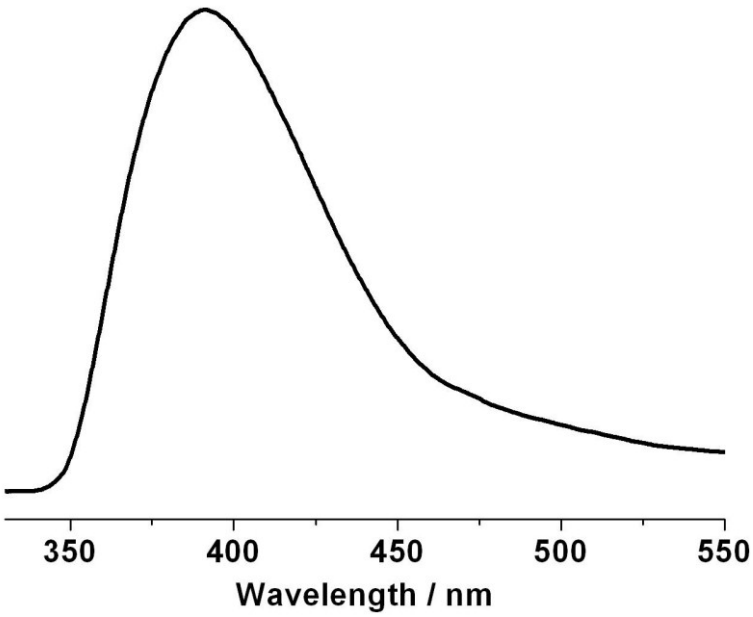

Figure S47. Emission spectra of the free ligand pytpy in solid state.

The detail of XPS spectra of 1, 1'-F, 1'-Cl, 1'-Br, 1'-I, and 1'-SCN

Complex **1**

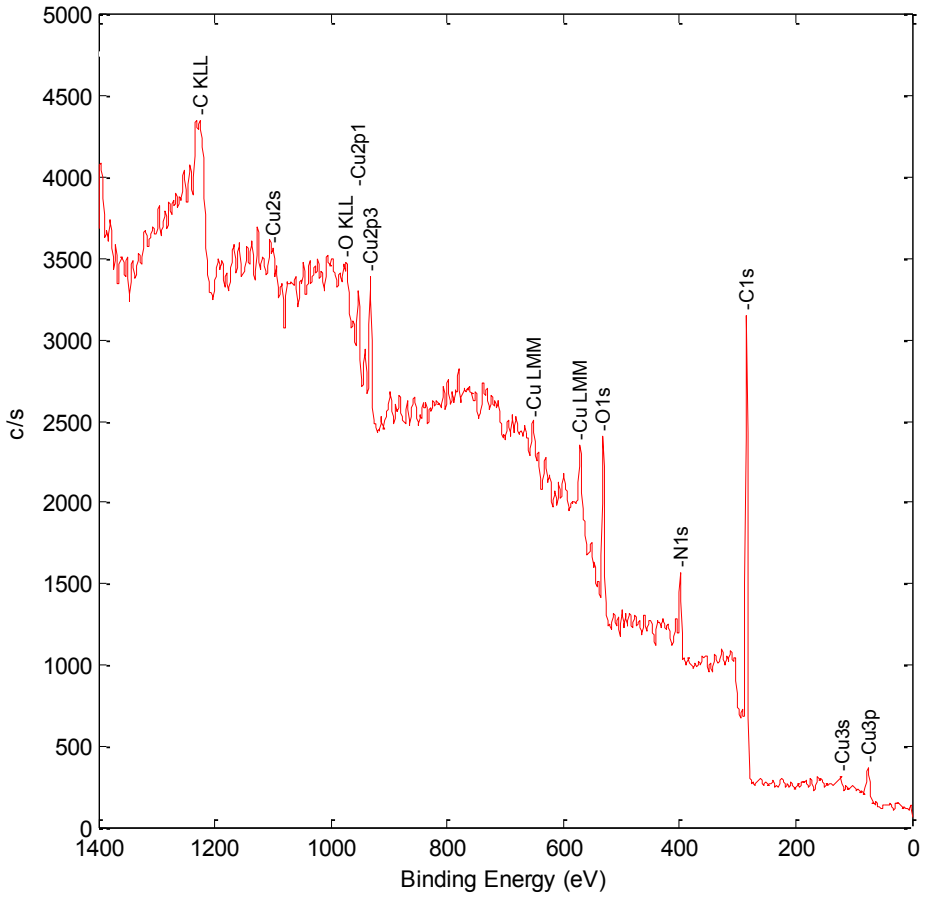

Element	Cu2p3
Relative atomic ratio (%)	1.87
Binding energy (eV)	932.37

Complex **1'**-F

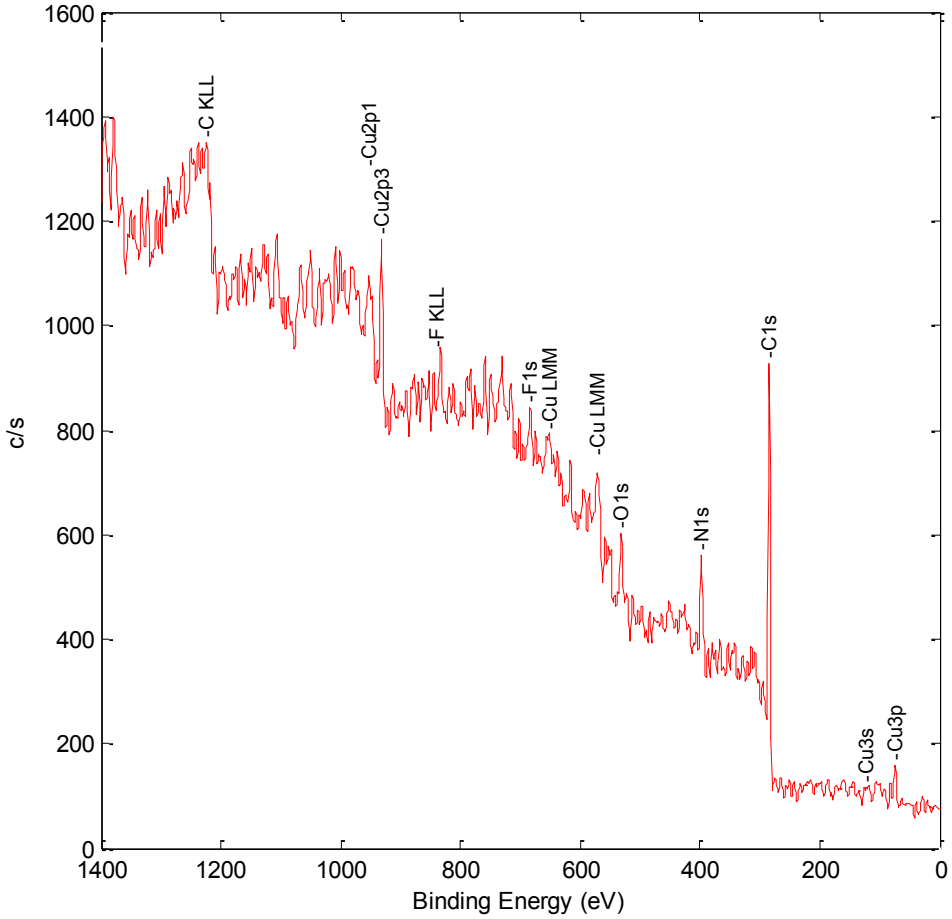

Element	F1s
Relative atomic ratio (%)	3.41
Binding energy (eV)	684.40

Complex **1'**-Cl

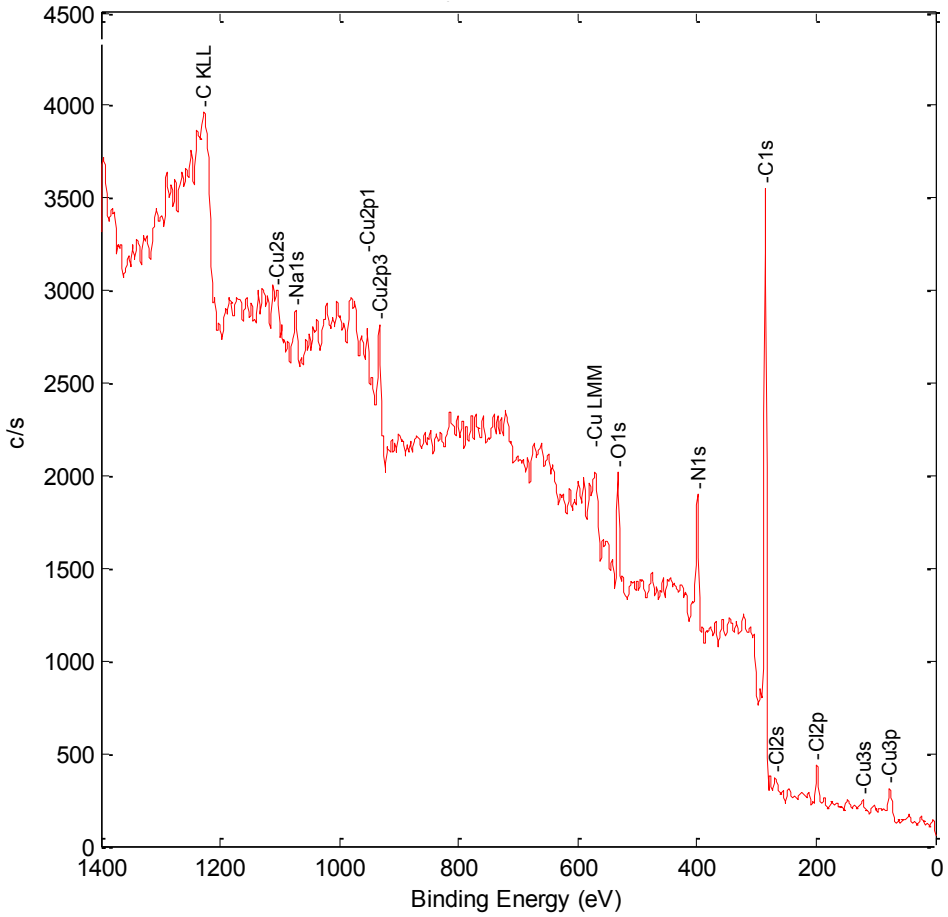

Element	Cl2p
Relative atomic ratio (%)	2.11
Binding energy (eV)	197.82

Complex **1'**-Br

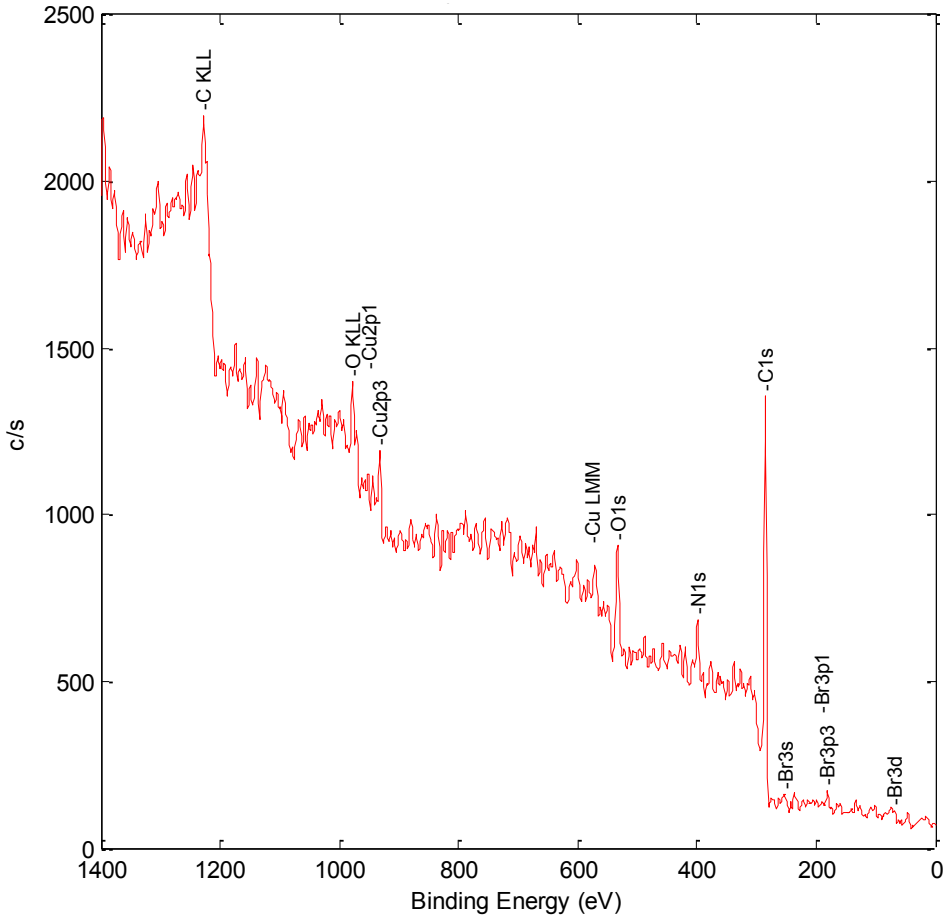

Element	Br3d
Relative atomic ratio (%)	1.64
Binding energy (eV)	67.49

Complex **1'**-I

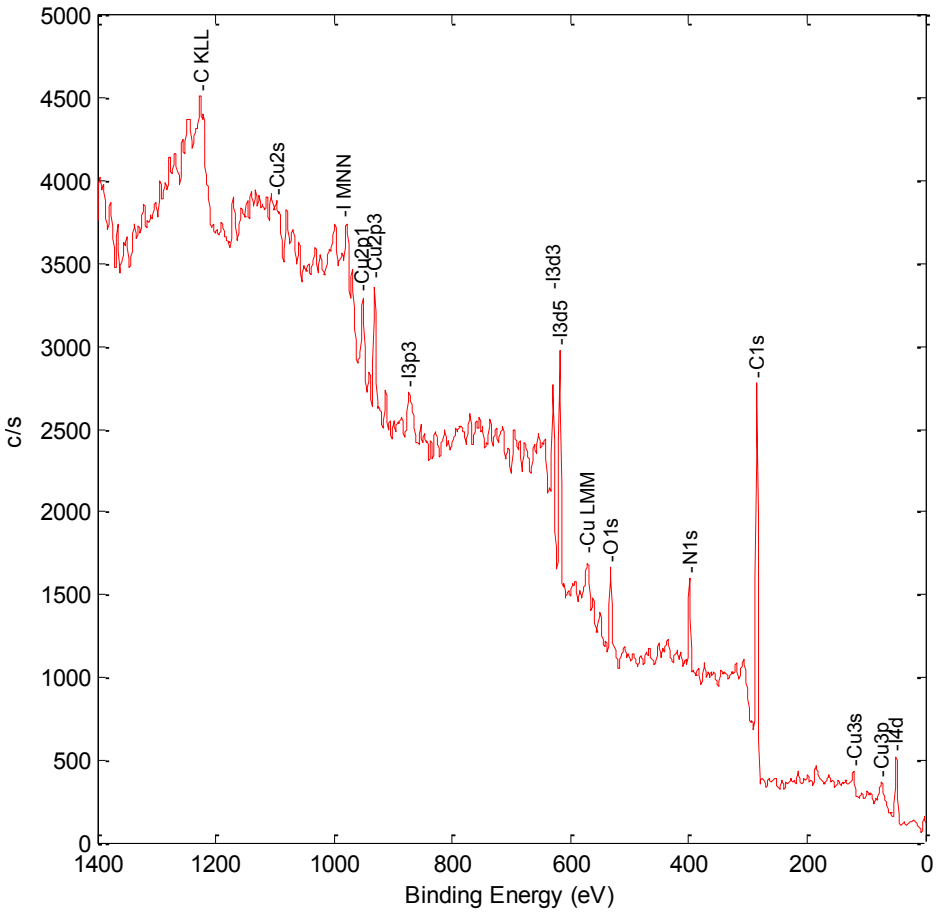

Element	I3d5
Relative atomic ratio (%)	1.93
Binding energy (eV)	618.30

Complex **1'**-SCN

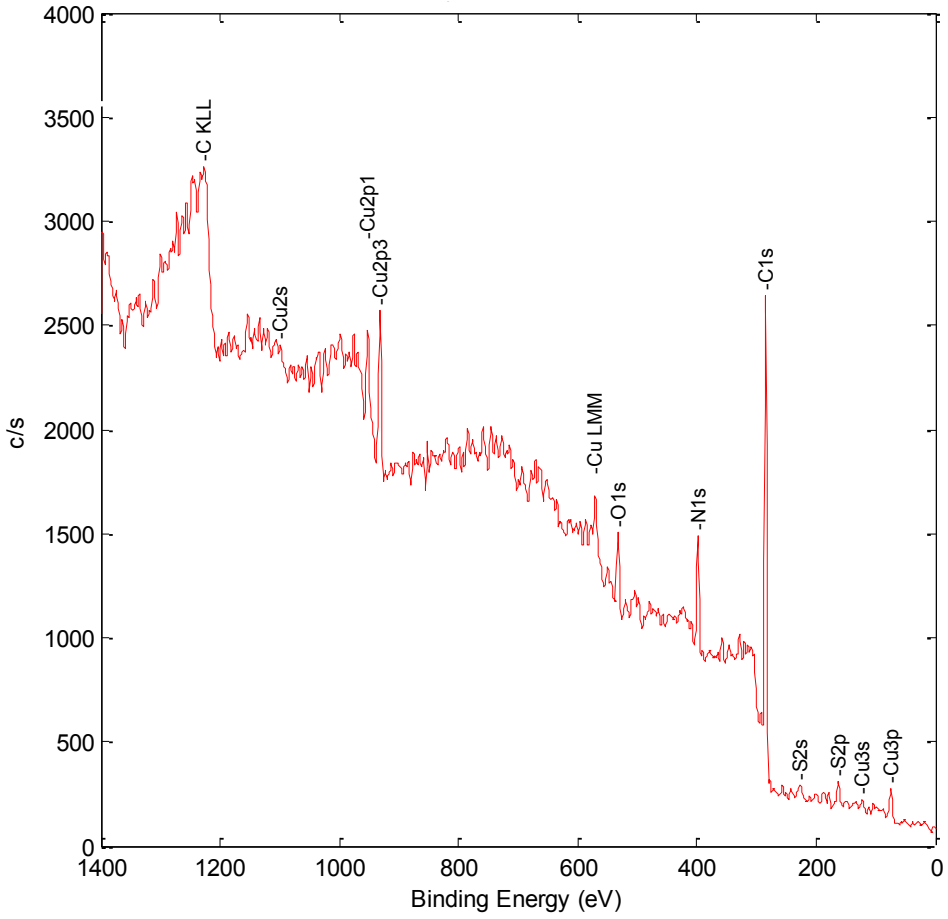

Element	S2p
Relative atomic ratio (%)	1.81
Binding energy (eV)	162.65

Table S1. Crystal data and structure refinement summary for complexes **1**, **1'**, and **1a**.

	1	**1'**	**1a**
Formula	$C_{21}H_{18}N_5O_4Cu$	$C_{20}H_{16}N_5O_4Cu$	$C_{21}H_{18}N_5O_4Cu$
fw	467.95	453.92	467.95
Temperature	293(2) K	293(2) K	293(2) K
Space group	$P2_1/c$	$P2_1/c$	$P2_1/c$
a [Å]	9.876(2) Å	9.399(19)	9.930(2)
b [Å]	9.295(1)	9.848(2)	9.3445(19)
c [Å]	22.594(6)	21.834(4)	22.717(6)
β [°]	106.80(3)	102.09(3)	106.94(3)
V (Å ^{3})	1985.6(8)	1976.2(7)	2016.5(8)
Z	4	4	4
F(000)	960	928	960
μ/mm^{-1}	1.140	1.143	1.123
R/wR $[I>2\sigma(I)]$ [a]	0.0938 / 0.1930	0.0955 / 0.2114	0.1033 / 0.2001
GOF on F^2	1.083	1.056	1.028

Table S2. Selected bond distances (Å) and angles (°) for complexes **1**, **1'**, and **1a**.

1			
Cu(1)-N(1)	1.991(6)	Cu(1)-N(2)#2	2.037(6)
Cu(1)-N(3)#1	1.964(6)	N(3)#1-Cu(1)-N(1)	126.8(3)
N(3)#1-Cu(1)-N(2)#2	123.4(2)	N(1)-Cu(1)-N(2)#2	109.8(2)
1'			
Cu(1)-N(1)	1.973(6)	Cu(1)-N(2)#2	2.081(7)
Cu(1)-N(3)#1	1.993(7)	N(1)-Cu(1)-N(3)#1	134.9(3)
N(1)-Cu(1)-N(2)#2	121.4(3)	N(3)#1-Cu(1)-N(2)#2	103.7(3)
1a			
Cu(1)-N(1)	1.981(7)	Cu(1)-N(2)#1	1.984(8)
Cu(1)-N(3)#2	2.020(8)	N(1)-Cu(1)-N(2)#1	126.3(3)
N(1)-Cu(1)-N(3)#2	123.6(3)	N(2)#1-Cu(1)-N(3)#2	110.0(3)

*Symmetry modes: **1**: #1 x+1, -y-1/2, z+1/2, #2 x, -y+1/2, z+1/2; **1'**: #1 x-1,-y+1/2, z-1/2, #2 x-1, y-1, z; **1a**: #1 x-1,-y+1/2,z-1/2, #2 x-1,y-1,z.